Astron. Astrophys. 327, 265–272 (1997)

ASTRONOMY
AND
ASTROPHYSICS

A spectral analysis of HDE 269445 from optical and infrared observations⋆

A. Pasquali[1], **W. Schmutz**[2], **A. Nota**[1,⋆⋆], **and L. Origlia**[3]

[1] Space Telescope Science Institute, 3700 San Martin Drive, Baltimore, MD 21218, USA
[2] Institut für Astronomie, ETH-Zentrum, CH-8092 Zürich, Switzerland
[3] Osservatorio Astronomico di Torino, Italy

Received 23 December 1996 / Accepted 9 May 1997

Abstract. We present new, near-IR spectroscopic observations of HDE 269445, which we combine with published *HST* and IUE ultraviolet data and optical high resolution spectra. We discuss the spectral morphology of the star from UV to near-IR wavelengths, concentrating on profile variations in the UV and optical H and He lines. From a spectroscopic analysis with non-LTE model atmospheres, we derive for HDE 269445: $T_\star$ = 34000 K, $R_\star$ = 43 $R_\odot$, log$\dot{M}$($M_\odot$/yr) = -4.5 and He/H = 0.4/0.6 by number. These parameters are in good agreement with those previously derived by Pasquali et al. (1997) who used only ultraviolet and optical lines. Therefore, our analysis confirms that a combination of optical and infrared lines can be fruitfully used to determine stellar and wind properties when ultraviolet data are not available.

Our model calculations only fit the broad component underneath a strong core emission. We interpret the discrepancy between the observed and the model line profiles as the effect of a non-spherical wind which has a hot, fast polar component and a cold, slow equatorial component. The time-variability detected in some H and He lines indicates that the wind geometry may be variable and the star has undergone changes in T_{eff} and $\dot{M}$. These properties are similar to those observed for the galactic LBV AG Carinae by Leitherer et al. (1994) and we may suspect that HDE 269445 is also a Luminous Blue Variable. This could explain why HDE 269445 has defied easy spectral classification, and, although originally classified as a Ofpe/WN9, it has always represented a peculiarity for this spectral type.

Key words: stars: atmospheres – mass-loss – early-type – Wolf-Rayet – HDE 269445 (LMC)

Send offprint requests to: A. Pasquali

⋆ Based on observations obtained at the European Southern Observatory, La Silla

⋆⋆ Affiliated with the Astrophysics Division, Space Science Department of the European Space Agency

1. Introduction

HDE 269445 (= S30 = R99 = BE261, hereafter R99) belongs to the Large Magellanic Cloud (LMC) and is embedded in a region of extended Hα emission, as it can be easily seen in the deep Hα + [N II] atlas of Davies, Elliott, & Meaburn (1976). On the basis of its spectral morphology, Walborn (1982) classified R99 as an Ofpe/WN9 star. So far, ten Ofpe/WN9 are known in the LMC. Their spectra are characterized by the simultaneous presence of low and high ionization emission lines at the same intensity (cfr. Bohannan & Walborn 1989). In fact, they present NIII and HeII emissions, which are typical of Of stars, and NII and HeI emissions, which are observed in spectral types later than WN7.

Extensive spectroscopic observations have been performed in the optical and ultraviolet to study in more detail the nature and the evolutionary role of Ofpe/WN9 stars. Recently, Crowther & Smith (1997) have suggested that, while massive O stars evolve directly into WN6 - WN7 stars, the less massive ones experience a Luminous Blue Variable stage (LBV), and, when quiescent, display Ofpe/WN9 characteristics. From an observational point of view, LBVs are characterized by high spectro-photometric variability which takes place over timescales of decades, and high mass loss (i.e. $\dot{M} \simeq 10^{-4}$ $M_\odot$ yr^{-1}in the case of AG Carinae, cfr. Leitherer et al. 1994). From an evolutionary point of view, the LBV phenomenon has been identified as the latest hydrogen burning stage, through which massive stars ($\sim 60\ M_\odot$) reduce their mass up to 50% of their initial mass and evolve into the WR phase (Langer et al. 1994).

The link between Ofpe/WN9 stars and LBVs is supported by the observations by Stahl et al. (1983), which followed the transformation of the prototype Ofpe/WN9 star R127 (in the LMC) into a LBV on a timescale of few years; and again by Stahl (1987), who found that the well known galactic LBV AG Carinae displays, during its high-temperature (or quiescence) stage, the typical spectral properties of an Ofpe/WN9 star. Recently, during a high resolution, spectroscopic survey of Ofpe/WN9 stars in LMC, Nota et al. (1996) have detected the presence of cir-

cumstellar nebulae around several Ofpe/WN9 stars, similar to those observed surrounding LBVs. They stated that this finding gives further strength to the connection between LBVs and Ofpe/WN9 stars.

HST/FOS ultraviolet observations have been used by Pasquali et al. (1997) to investigate the evolutionary status of the LMC Ofpe/WN9 stars. The stellar and wind parameters, as derived from the UV spectral analysis, have been used to place the Ofpe/WN9 stars on the HR Diagram and to perform a direct comparison with the present, available evolutionary tracks. Pasquali et al. have found that both higher mass-loss rate (during the main-sequence evolution) and enhanced mixing between stellar core and envelope are required in order to match the models with the observed Ofpe/WN9 stellar properties. The following evolutionary sequence has been then proposed: O – Of – H-rich WNL – Ofpe/WN9, where the Ofpe/WN9 phase is still supported by hydrogen burning for initial stellar masses less than $\sim$ 100 $M_{\odot}$. The Ofpe/WN9 phase appears also to be characterized by highly reduced surface H mass fractions (X_S from 0.5 down to 0.3) which are comparable to the X_S values measured in LBVs by Crowther et al. (1995).

The class of Ofpe/WN9 has been further divided by Walborn (1977) and, subsequently by Bohannan & Walborn (1989), into three subcategories, depending on the spectral morphology in the Hδ region. The R127 subcategory includes stars which show narrow SiIV λ4089 and NIII λ4097 in absorption. BE294, S119, S9 and S61 belong to this group. The R84 class is characterized by the presence of P Cygni profiles in the above lines, and includes HDE 269927c and BE381. Finally, the R99 class lists only R99, in virtue of the fact that no absorption is present in its spectrum except, maybe, a diffuse, weak absorption at NIII λ4097. In particular, Walborn (1977) points out that, given the low-excitation emissions in its spectrum, R99 resembles a B-type P Cygni star. On the other hand, its HeII λ4686 emission is typical of Of stars.

Bohannan & Walborn's (1989) sub-classification has been also confirmed by Pasquali et al.'s (1997) analysis at λ = 1300 Å, 1950 Å and 2070 Å. These spectral regions are dominated by NiV, NiIV, FeIV and FeIII absorptions, which appear to be stronger in the spectra of BE294, S119, S9. The same lines are less pronounced in the spectra of the stars belonging to the R84 class, such as HDE 269927c and BE381. Finally, the Ni-Fe features are nearly absent in the spectrum of R99.

A number of important differences between R99 and the remaining of the Ofpe/WN9 class has been pointed out so far. Nota et al. (1996) showed that the energy distribution of R99 is characterized by the strongest infrared excess among the Ofpe/WN9 stars, which can be explained via free-free emission by a very massive wind. In addition, Pasquali et al. (1997) and Crowther & Smith (1997) have discussed the peculiar UV blanketing pattern of R99, which is due to iron at a higher ionization degree than that of the other Ofpe/WN9 stars. They have also noticed the absence of blue-shifted absorptions in the optical HeI lines compared to P Cygni profiles with well developed absorptions troughs observed in the other Ofpe/WN9 stars, and the evidence that the stellar wind in R99 is characterized by a higher (almost a factor of 2) terminal velocity with respect to the rest of Ofpe/WN9 stars. Crowther & Smith (1997) have discussed the shallow, violet absorption in the HeI P Cygni profiles of R99 blue-shifted by 1050 km/s, compared with the sharp P Cygni profiles observed in other Ofpe/WN9 stars, and the asymmetric profile of the HeII λ4686 line. These authors have also noted an overall optical and near-infrared spectral similarity of R99 to the LBV candidate HD5980 in the SMC in December 1994. The possibility that R99 could be a binary system is mentioned by Walborn (1977); moreover, R99 has been suggested as the optical counterpart for LMC X-5 by Byrne (1975).

In order to clarify the nature and the stellar properties of R99, we have undertaken a detailed analysis of some H and He diagnostic lines. In Sect. 2 we present the data and in Sect. 3 we discuss the observed spectral morphology of R99. In Sect. 4 we describe the spectral analysis developed in order to derive the stellar parameters of R99; discussion and conclusions follow in Sect. 5.

Table 1. IR spectroscopic observations

Spectral range (μm)	Observed line (μm)
1.0759 – 1.0898	HeI λ1.083
1.2506 – 1.2628	HeI λ1.25
1.2759 – 1.2877	Pβ
1.6271 – 1.6599	Br 12 - 4
2.0438 – 2.0726	HeI λ2.058
2.1528 – 2.1812	Brγ

2. The data

We observed R99 in December 1994 at ESO, La Silla, with the infrared spectrograph IRSPEC (Moorwood et al. 1991), mounted on the NTT 3.5m telescope. Our selected spectral ranges are listed in Table 1.

The spectral resolution in these configuration is given by the line FWHM (10 Å) which corresponds to a $\lambda/\Delta\lambda$ of $\sim$ 1200, 1600 and 2200 in the J, H and K bands, respectively.

We observed in sequences of object - sky pairs, usually selecting DIT = 60 s and NDIT = 5. The total integration time on source ranged between 12 and 25 minutes, depending on the selected grating position. The sky frames were acquired at 40" south of R99. We also acquired flat-fields using a halogen lamp and bias frames. We observed the standard star BS 2882 in oder to flux-calibrate our data.

Data reduction was performed using the IRSPEC context inside MIDAS, the ESO standard reduction package. Each frame was sky subtracted using the nearest-in-time sky frame. Flat-field correction and wavelength calibration were then applied through the on–line calibration pipeline of the instrument. The final one-dimensional spectra were obtained extracting the central 5 rows of the long slit frames which correspond to a slit aperture of 4.4" x 11".

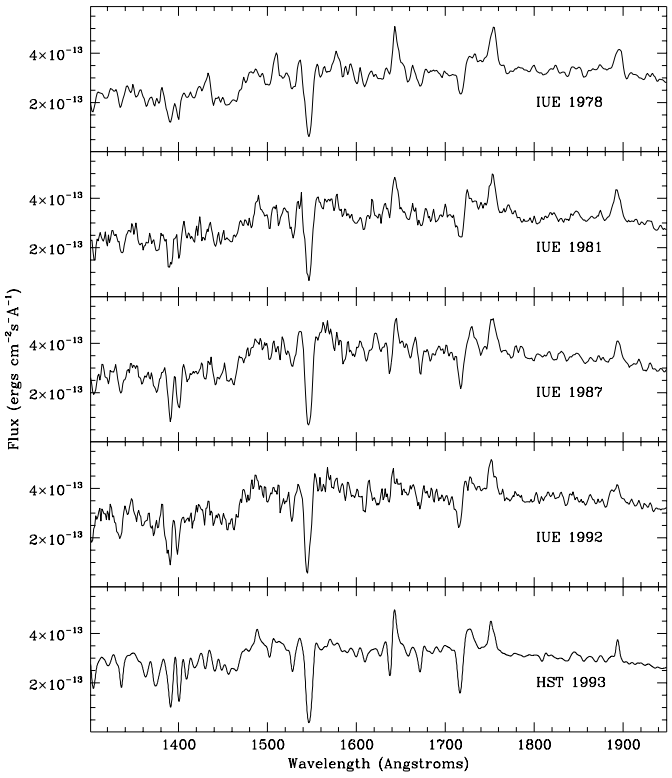

Fig. 1. The UV spectrum of R99, between 1300 Å and 1950 Å, in the years 1978, 1981, 1987, 1992 (IUE observations) and 1993 (*HST* acquisition). The latter has been rebinned in order to be comparable with the IUE resolution.

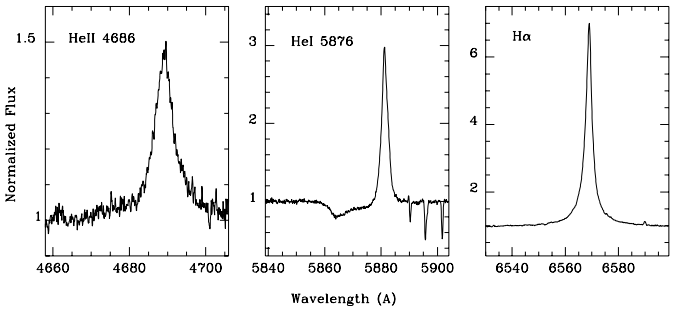

Fig. 2. HeII λ4686, HeI λ5876 and Hα line profiles. The continuum has been normalized to unity in order to easily compare the lines shape.

We have complemented the infrared spectra with the optical Hα, HeII λ4686 Å and HeI λ5876 Å lines, collected from the database of Nota et al. (1996) and for which we performed a more careful nearby continuum level normalization. These data come from a high resolution (R $\simeq$ 20000), echelle spectroscopy study of a large sample of Ofpe/WN9 stars in the LMC, that Nota et al. (1996) have obtained in order to study in details the Ofpe/WN9 optical H and He line profiles.

We have also collected all the IUE and *HST* ultraviolet spectra available for R99 from the archives. In the case of IUE, observations were taken in 1978, 1981, 1987 and 1992 by PIs Hutchings, Shore, Bohannan and Howarth with the low dispersion camera coupled with the large aperture. The *HST/FOS* UV observations have been obtained by Leitherer (proposal-ID 4260 and 5702) and are described in Pasquali et al. (1997).

3. The spectra

The UV spectra are plotted in Fig. 1, where the HST spectrum (lower panel) has been rebinned in order to match the lower IUE spectral resolution.

Remarkable are the variations occurring in the spectral range between 1600 Å and 1800 Å which includes the HeII λ1640 and NIV λ1718 lines. The HeII λ1640 appears to switch on and off: in the 1978 and 1981 spectra it is mostly present in emission, even if a weak absorption can be detected in the raw image of the 1981 spectrum. On the contrary, in the 1992 data the line emission is significantly reduced. HeII λ1640 switches on dramatically in the 1987 and 1993 spectra, where it shows a strong and well defined P Cygni profile. NIV λ1718 is almost constant in 1978, 1981 and 1992, with a developed absorption and a weak emission component. Only in the 1987 and 1993 data its emission becomes pronounced. The observed line variations do not, however, affect significantly the continuum distribution of R99 which has remained nearly identical over a period of 15 years. The 1993 HST/FOS spectrum of R99 nicely resembles, in terms of the HeII λ4686 profile, the star HD93131 classified either WN6-A by Walborn et al. (1985) or WN7-abs by Crowther et al. (1995), and therefore supports the suggestion of an earlier WN spectral type for R99.

The optical lines (HeII λ4686 Å, HeI λ5876 Å and Hα, observed in 1991) are shown in Fig. 2, while the infrared lines (observed in 1994) are to be found in Fig. 3, following the order: HeI λ1.083 μm, HeI λ1.25 μm, Pβ, Br 12-4 λ1.64 μm, HeI λ2.058 μm and Brγ. Their adjacent continua have been normalized to unity.

Although the optical and infrared observations were not taken during the same year, we still can compare their profiles (in Figs. 2 and 3) and immediately note the striking similarity of the HeI λ5876 Å, HeI λ1.083 μm and HeI λ2.058 μm profiles. The lines are all characterized by a prominent emission which is "detached" from the absorption component of the profile. The latter is blue-shifted of $\sim$ 1000 km/s and its intensity is $\sim$ 50% of the continuum level. The line width of the emissions reflects expansion velocities of $\sim$ 400 km/s (Nota et al. 1996). Due to the low S/N ratio of the data we are not able to detect any P Cygni profile in HeI λ1.25 μm (which corresponds to the transition 4^3P – 3^3S) and in HeI λ2.16 μm (from the transition 7^3F – 4^3D), which is blended with the Brγ line. HeII lines are identified at λ = 1.64 μm (the HeII 24-8 line in blend with the Br 12-4 emission) and λ = 2.16 μm (the HeII 14-8 feature which seems partially resolved from the Brγ line). Since they are blended with H lines, we cannot compare their profiles with that of the optical HeII λ4686 Å line. The latter is formed by a broad emission with an intensity of $\sim$ 50% of the continuum level. The presence of a red wing of emission makes the HeII λ4686 profile slightly asymmetric. All H and He lines

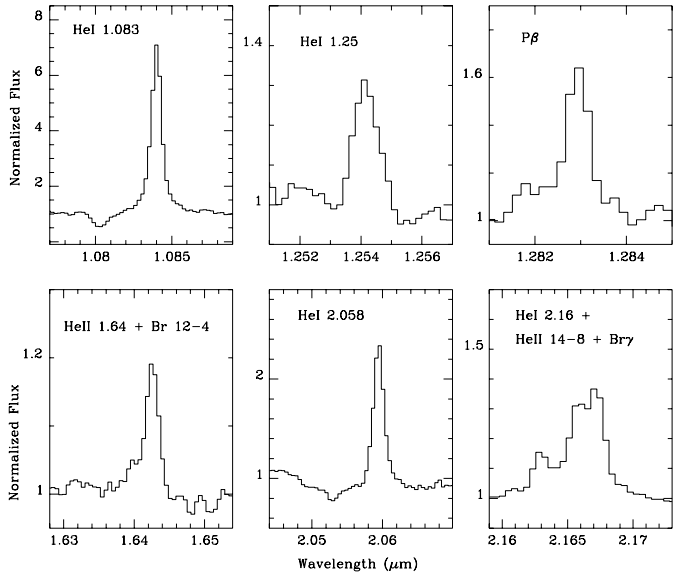

Fig. 3. New observations of the infrared spectrum of R99. They include the lines: HeI λ1.083 μm, HeI λ1.25 μm, Pβ, HeII λ1.64 μm, HeI λ2.058 μm, HeI λ2.16 μm and Brγ.

Table 2. Equivalent widths in Å

Line	
HeII λ 4686 Å	-2.5
HeI λ 5876 Å	-5.5
	1.8
Hα	-24.7
HeI λ1.083 μm	-20.6
	3.1
HeI λ1.25 μm	-3.0
Pβ	-3.0
HeII λ1.64 μm	-0.8
Br 12-4	-4.0
HeI λ2.058 μm	-5.6
	1.2
HeI λ2.16 μm	-2.0
HeII 14-8	-5.0
Brγ	-4.0

have emissions that are comparable in width. In addition, the Hα line shows weak wings, at both the red and the blue side, that extend to $\sim$ 1000 km/s. The lower resolution of our infrared spectra does not allow us to detect the presence of such wings in the Pβ and Brγ lines.
The equivalent width of all the optical and infrared lines in Figs. 2 and 3 are reported in Table 2. Negative values refer to emission features, while positive values are derived for absorption lines. The Hα equivalent width is sligthly higher than that measured by Nota et al. (1996), since we have here taken into account the line wings.

4. The spectral analysis

The H and He lines presented in Figs. 2 and 3 are commonly used to determine the stellar properties. Their profiles are the *fingerprints* of specific stellar parameters, such as $T_\star$ and the He/H abundance ratio, and of specific stellar wind properties, such as the wind density, V_∞ and the velocity law. The comparison of the observed line profiles with the synthetic ones (calculated by assuming *a priori* a particular set of values for $T_\star$, V_∞, β, the power index of the wind velocity law, and He/H ratio), allows us to derive the stellar characteristics of R99.

We have calculated a grid of spherically expanding atmosphere models with a line blanketing, non-LTE code, that combines the "Kiel atmosphere" with the line blanketing treatment of Schmutz (1991). The models assume spherically symmetric outflows. The radiation transfer of the lines is treated in the comoving frame and the continuum is blanketed by the presence of tens of thousand lines. The non-LTE rate equations are solved for 11 hydrogen levels and 28 helium levels (Wessolowski et al. 1988). A more detailed description of the code can be found in Schaerer & Schmutz (1994). In addition, we have used a constant photon loss factor of 10^{-4} to account for the interaction of the HeII λ303 Å resonance line with metal transitions (cf. Schmutz 1997). The grid spans a temperature range of 29000 K to 40000 K and a range in mass loss from 10^{-5} to 10^{-4} $M_\odot$ yr^{-1}, and has been calculated also for different terminal wind velocities and different exponents of the β - law that we assumed to represent the wind velocity law (Hamann & Schmutz 1987).

We have then produced theoretical line profiles, which have been convolved with the instrumental profile and compared to the observed H and He lines. An iterative procedure has allowed us to define the best model that fits the broad component in the observed line profiles.

The final fits are shown in Figs. 4, 5 and 6 for the HeII λ4686 Å, Hα and HeI λ1.083 μm lines, where the solid line is used for the observed profiles. All the synthetic profiles have been computed by assuming $T_\star$ = 34000 K, β = 0.5, V_∞ = 1000 km/s and He/H = 0.4/0.6 by number.

In Fig. 4 we have plotted the observed HeII λ4686 Å profile and superimposed on it three synthetic profiles resulting from models with different stellar temperature. The dot-dash profile represents the final model at $T_\star$ = 34000 K and T_{eff} = 31600 K, which is in good agreement with the observed line even if it slightly underestimates the blue edge of the line. The dotted profile has been, instead, calculated for a $T_\star$ of 33000 K; as we can easily see, it fails to reproduce the emission peak of the observed HeII λ4686, thus indicating a higher stellar temperature. Finally, the dashed contour represents the theoretical HeII λ4686 line at $T_\star$ = 35000 K. In this case, the synthetic profile overestimates the red edge and the flux peak of the line, indicating that the assumed temperature is too high. In Fig. 5 we have compared the observed Hα with fits obtained for different $\dot{M}$ values, and the same $T_\star$ value of 34000 K. The dot-dash profile represents the best fitting model and, indeed, reproduces quite well the weak wings of the observed line. The dotted profile has been determined by assuming a mass loss rate higher by 0.1 dex.

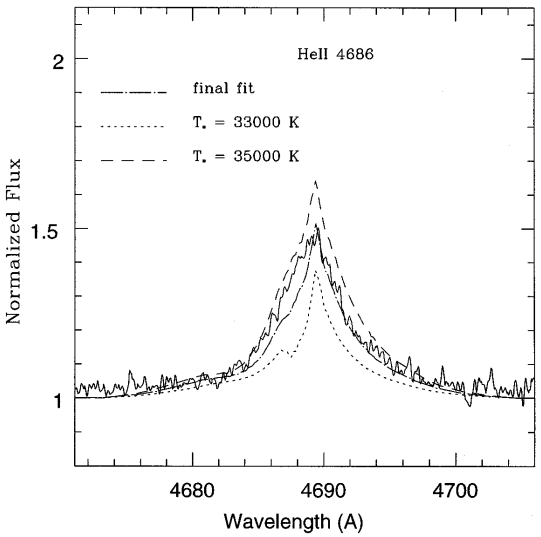

Fig. 4. HeII λ4686 fits. The solid line represents the observed line profile, while the dot-dash profile is our best model fit. The short and long dash profiles have been calculated for $T_\star$ = 33000 K and 35000 K, respectively.

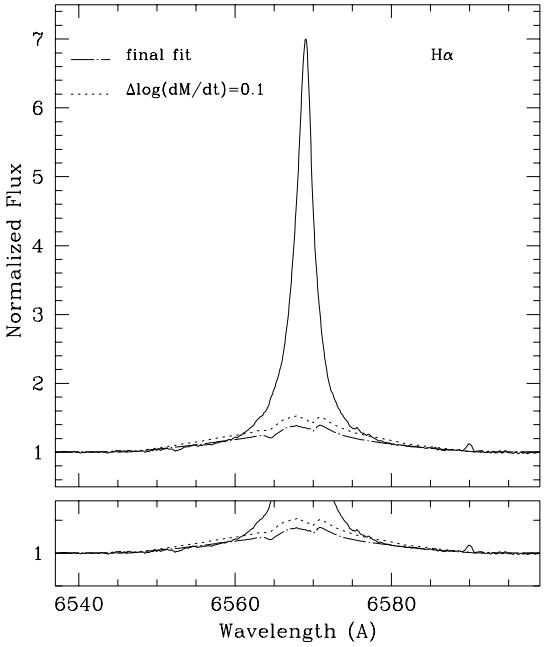

Fig. 5. Hα fits. The solid line represents the observed line profile, and the dot-dash profile is our best model fit. The short dash profile has been computed assuming a 0.1 dex higher mass loss rate.

The effect of a higher mass-loss rate is to increase the flux peak of the Hα emission together with the emission in the line wings. Finally, Fig. 6 superimposes the observed HeI 1.083 μm line on the synthetic profiles computed for different β values.

The dot-dash profile, which has been calculated with $\beta = 0.5$, nicely reproduces the observed absorption feature whereas the $\beta = 1$ profile yields a stronger absorption than detected. Clearly, our technique is able to fit only the component which accounts for the absorption and the weak and broad wings of emission in the line profiles. It fails to reproduce the peak of the Hα and HeI λ1.083 μm emissions; we will later discuss the origin of this second, narrower component. Meanwhile, from the absorption profile fits and the HeII λ4686 fits, we derive: $T_\star$ = 34000 K and T_{eff} = 31600 K (the photospheric temperature at the radius where Rosseland $\tau = 2/3$), V_∞ = 1000 km/s, and He/H = 0.4/0.6 by number. The radius and the mass loss rate cannot be derived from the spectrum but only the ratio $\dot{M}/R_\star^{3/2}$ (cf. Schmutz et al. 1989). The procedure followed to derive $\dot{M}$ and $R_\star$ is discussed below. The internal precision associated with the derived values can be estimated by comparing the different profiles synthetised for each lines. We have used the above stellar parameters in order to compute the theoretical, astrophysical fluxes in the U, B and V bands, and the theoretical Spectral Energy Distribution (SED) from UV to IR wavelengths. We have compared the theoretical with the observed SED (Nota et al. 1996; Pasquali et al. 1997) in order to estimate the stellar radius and reddening of R99. In fact, by superimposing the two SEDs at the V magnitude (we have avoided the K magnitude since R99 shows a strong infrared excess), we have determined the scaling factor of the theoretical to the observed SED, which is a function of the distance, radius and reddening of R99. In order to quantify the reddening, we have adopted the galactic extinction law from Seaton (1979) and Howarth (1983) and, for the LMC extinction law, the extinction law derived by Fitzpatrick (1986) for 30 Dor. An E(B-V)$_{GAL}$ around 0.1 mag coupled with an E(B-V)$_{LMC}$ of 0.12 mag does not properly match the modelled SED to the observed one.

According to Fig. 7, such a correction (which corresponds to the dashed line) makes the spectral feature at λ = 2200 Å too strong. In order to avoid this effect, a very high reddening in correspondance with the spectral bump at λ = 1200 Å or, alternatively, a steeper extinction law should be adopted. On the other hand, there is no observational evidence for extinction laws steeper than that derived for 30 Dor and a higher reddening would increase the infrared excess in the energy distribution of R99. Our best fit (the solid line in Fig. 7) is then given by E(B-V)$_{GAL} \simeq 0.03$ mag and E(B-V)$_{LMC} \simeq 0.24$ mag, which yield a total reddening of 0.27 mag, a stellar radius of 43 $R_\odot$, log($L/L_\odot$) = 6.2 and log$\dot{M}$($M_\odot$/yr) = -4.5 at the assumed LMC distance of (m-M_V) = 18.55 mag (Panagia et al. 1991).

Our profile-fitting technique yields $T_\star$, $R_\star$ and L in agreement with the values derived by Pasquali et al. (1997) who based their analysis on line equivalent width. In this work, we determine a higher mass-loss rate (of a factor of $\sim 20\%$) and a lower reddening (of about 0.1 mag). While Pasquali et al. made use of ultraviolet and optical lines, we have analysed optical and infrared features. Therefore, the agreement between the results of these two works confirms the self-consistency of our fitting procedure and shows that a combination of optical and infrared lines can be used to diagnose stellar parameters when ultraviolet data are not available. A refinement of this procedure in order to derive stellar properties only from infrared lines (in the case of heavily extincted objects) is in progress.

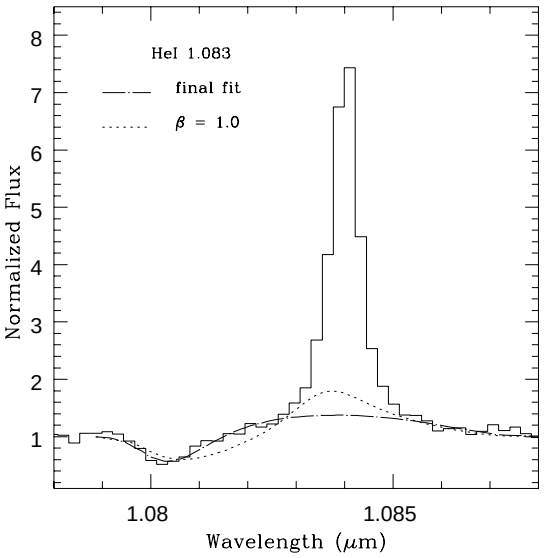

Fig. 6. HeI λ1.083 μm fits. The solid line represents the observed line profile, and the dot-dash profile is our best model fit. The short dash profile has been derived using a velocity law power index, β, of 1.

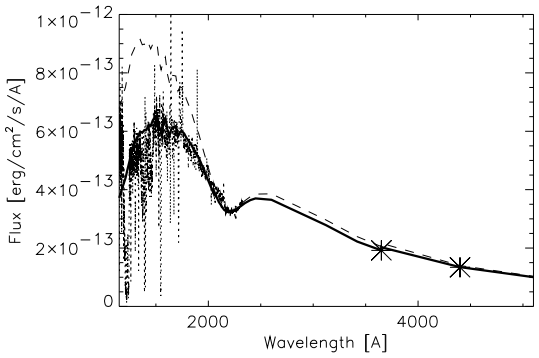

Fig. 7. R99 spectral energy distribution from UV to the V band. The dashed fit represents the theoretical SED reddened with E(B-V)$_{GAL} \simeq$ 0.1 mag and E(B-V)$_{LMC}$ = 0.12 mag. The solid curve is instead the theoretical SED reddened with E(B-V)$_{GAL} \simeq$ 0.03 mag and E(B-V)$_{LMC}$ = 0.24 mag. We have here assumed the galactic extinction law by Seaton (1979) and Howarth (1983), while we have adopted for the LMC extinction law the law derived by Fitzpatrick (1986) for 30 Dor.

5. Discussion and conclusions

Previous infrared, spectroscopic observations of R99 were carried out by McGregor et al. (1989) and Morris et al. (1996). McGregor et al. data, acquired with a resolution power R $\simeq$ 450, show a weak P Cygni profile in the HeI λ2.058 μm line and also the presence of the HeI λ2.11 μm. They did not resolve the HeII 14-8 – Brγ blend. The authors gave a HeI2.058/Brγ flux ratio of 4, from which they derived a He/H abundance ratio (by number) larger than 0.5. Our spectra indicate a HeI2.058/Brγ flux ratio of 3.5 and our spectral analysis gives a He/H ratio of $\sim$ 0.7, in agreement with McGregor et al.

A more extended infrared spectrum has been taken by Morris et al. (1996). It covers the spectral range between 1.45 and 1.80 μm at R $\simeq$ 550, which is characterized by the HI Brackett series, and the spectral interval between 2.0 and 2.3 μm, where, again, the HeII 14-8 and the Brγ lines are not resolved. From the comparison with other Ofpe/WN9 and LBV stars the authors have suggested that R99 could be a LBV object in eruption since the strength of its HeI λ2.058 μm is comparable to that observed in LBVs.

The variability of the HeII λ1640 line, in equivalent width and profile, seems to support the suggestion of Morris et al. The spectra collected in Fig. 1 indicate that R99 temperature and wind density change over timescale as short as one year at least. Stellar atmosphere models indicate that the continuum slope between 1200 Å and 3000 Å is not sensitive to temperature variations at T$_\star$ > 30000 K. They also point out that the continuum absolute flux should vary with T$_\star$ at constant luminosity, so that an increase of 10000 K would make the continuum brighter by about 1 mag (at UV and optical wavelengths). On the contrary, at T$_\star$ > 30000 K, the HeII lines are very sensitive to small changes in T$_\star$. Since the continuum in R99 has been constant within the measurement uncertainty of IUE, we then suspect that R99 has experienced small temperature variations. In fact, Fig. 4 shows that a variation of 2000 K in the stellar temperature (from 33000 K to 35000 K) produces a variation of a factor 2 in the emission of the HeII λ4686 line. This applies as well to the HeII λ1640 line; since we can observe nearly a factor of 2 change in the HeII λ1640 emission in Fig. 1, we may estimate a ΔT$_\star$ of few thousands degrees. These variations, together probably with wind density changes, may be responsible for the observed variations in the HeII λ1640 profile.

Unfortunately, a SIMBAD research through all the R99 data available in literature has shown that there are no optical spectra observed at the same IUE visit epochs, except for the 1978 observations by Walborn (1982), which would be useful to perform a homogeneous time - analysis of the R99 spectral variations from ultraviolet to optical wavelengths. However, we can look for optical variability, indipendently of the IUE data. A first set of optical spectra was taken by Stahl et al. (1985) in the years 1982, 1983 and 1984. In particular, Stahl et al. pointed out a factor of 2 variation in the line strength of the HeI λ4471 and Hγ. A closer look to their Fig. 6 reveals also a variation in the line profiles. In fact, the two lines seem to evolve from the 1982 symmetrical profile to a progressively asymmetrical shape, having a sharper blue edge and an extended, weak wing on the red side (in similarity with the HeII λ4686 line of Fig. 3). Since HeI λ4471 and Hγ are in emission and then originate in the wind, we might infer from their variability that some changes have occurred in the wind density and in the geometry of R99 stellar wind over a timescale of one year. We can then compare the data of Stahl et al. (1985) with the spectra subsequently taken by Bohannan & Walborn (1989), Nota et al. (1996) and Crowther & Smith (1997). First of all, the 1984 spectrum shows weak FeII emissions comparable to those present in the spectrum of the LBV R71, taken in the same epoch and during outburst. For the sake of comparison, the FeII lines appear with a P Cygni profile in R71 and completely in emission in R99. Stahl et al. (1985) identified also a weak emission of MgII λ4481 in the spectrum

of R99, which is generally due to a relatively cool and dense stellar wind. FeII and MgII lines have been no more detected in the subsequent observations of Bohannan & Walborn (1989) and Crowther & Smith (1997) [Nota et al. 1996 spectra did not achieve a good S/N ratio below $\sim$ 4300 Å]. Although the data are not systematic, they provide circumstantial evidence for changes in the wind properties of R99.

Optical and infrared H and He lines represent, when used together, a powerful tool to analyse the stellar and wind properties, since they sample different depths in the wind with respect to the stellar photosphere. By using the HeII λ4686 Å, Hα and HeI λ1.083 μm as inputs for our stellar atmosphere code we have derived for R99 $T_\star$ = 34000 K, T_{eff} = 31600 K, $R_\star$ = 43 $R_\odot$, log(L/$L_\odot$) = 6.2, log$\dot{M}$($M_\odot$/yr) = -4.5, He/H = 0.4/0.6 by number, and E(B-V) = 0.27 mag. The accuracy on the derived He/H ratio can be estimated in Fig. 5. The fits show that our mass loss rate is within 0.1 dex of uncertainty, or, alternatively, that the accurancy on the H content is 0.1 dex, at first order. Therefore, the internal precision of the H/He abundance is 0.1 by number or 25% in ratio. The theoretical fits to the observed lines are found in Figs. 3 to 5. It is clear from the figures that the parameters adopted in order to properly fit the HeII λ4686 Å emission and the HeI 1.083 μm absorption do not reproduce the Hα and HeI 1.083 emissions. Neither we can fit these emissions by varying the velocity law exponent β and the mass-loss rate. The subtraction of the synthetic profiles from the observed lines gives a residual emission which is characterized by a FWHM of $\sim$ 200 km/s in both Hα and HeI 1.083 μm. In the hypothesis that the residual emission is of nebular origin, we would conclude that the nebula is expanding at $V_{exp} \simeq$ 100 km/s. As an interesting comparison, the combined emission of the stellar wind and the circumstellar nebula has already been found in the spectrum of the massive YSO S106IR by Drew et al. (1993). This galactic object is the exciting source of the HII region Sh-2 106 which shows a striking bipolar geometry. Drew et al. have proposed that the low-contrast and high-velocity wings, seen in the Brγ, Brα and Pγ lines, are due to the stellar wind, while the narrower emission components are produced by the underlying HII region. In their case, the FWHM value of the narrower emission component indeed agrees with the nebular expansion velocity measured from the nebular Hα emission. In the case of R99, we also detect nebular, forbidden lines (cf. Nota et al. 1996). The histogram of the radial velocities obtained by Nota et al. (1996) by spatially sampling the Hα emission indicates that the underlying nebula (whether of stellar or interstellar origin is still not clear) is in expansion at 30 km/s. This is also confirmed by the FWHM value of the [NII] λ6584, [SII] $\lambda\lambda$6717 and 6731 Å lines (cf. Nota et al.'s Table 9). If the circumstellar matter were the source of the Hα and HeI 1.083 narrow emissions, these components should be characterized by a FWHM of $\simeq$ 30 km/s instead of 200 km/s or, alternatively, high-velocity components, comparable to V_R = FWHM/2 $\simeq$ 100 km/s, should also be detected in forbidden lines. Nevertheless, the [NII] and [SII] lines in R99 spectrum do show a systematic expansion velocity of 30 km/s. We may then infer that the observed, Hα and HeI 1.083 emission excess is intrinsic to the star.

In conclusion, we find a number of unanswered questions which can be summarized as follows:
i) the spectroscopic variability;
ii) the emission excess in the H and HeI lines with respect to the model predictions;
iii) the observed SED, whose model fitting over the whole UV - IR range results in an increasing observed, emission excess from the V to the K band.
Point *i)* may be explained in terms of wind density and effective temperature variations, while points *ii)* and *iii)* may well due to a non-spherical stellar wind. Following Zickgraf (1992)'s two-component wind model for B[e] stars, we may represent the wind in R99 as a combination of a fast wind located at the stellar poles and a slow wind in the equatorial plane. The UV measurements of CIV and SiIV lines and the optical detection of the HeII λ4686 allow us to characterize *only* the fast component emission. When we apply our wind model to the H and HeI lines we miss the major emission due to the slow and cold wind. In other words, the discrepancy between the theoretical and observed profiles of H and HeI lines would come from the model assumption of wind spherical symmetry and from fitting only the fast polar wind, which is defined by our UV and optical data. Furthermore, the emission excess detected in the V and infrared bands justifies the presence of a slow equatorial wind, whose higher density favour dust formation and free-free emission. Near-infrared excesses are commonly observed in Be stars and interpreted as arising from a high density, low velocity plasma in the equatorial plane of the star (Dougherty et al. 1994).

Support to our scenario is also given by the asymmetric profile observed for the Hγ and HeI λ4471 lines. Similar red wings have been previously detected in some H and HeI lines of BE381 and HDE 269927c by Nota et al. (1996) and BP Tau by Calvet & Hartmann (1992). In the latter case Calvet & Hartmann (1992) and Calvet, Hartmann & Hewett (1992) have been able to theoretically reproduce the red wing by assuming disklike and bipolar geometry of the circumstellar matter and stellar wind associated with BP Tau, respectively. More speculative is the comparison between the Hα profiles observed in R99 and those shown by Be - B[e] spectra. The inspection of Doazan et al. (1991)'s atlas reveals an interesting similarity between the Hα lines of R99 and HD217891 (and, more in general, HD120991, HD25940, HD32991, HD5394) characterized by a Vsin(i) of 100 km/s. A *caveat* has to be mentioned at this point: our fitting procedure has allowed us to derive the mass loss rate associated with the polar wind component through atmosphere models, where this component arises from the whole stellar surface. Since the real polar wind comes from half of the stellar surface at least, it is necessary to correct our mass loss rate by a factor 1.4 (the wind emission scales with square density) and increase our T_{eff} value of $\sim$ 2000 K in order to still reproduce the observed wind emission. Consequently, our derived log$\dot{M}$($M_\odot$/yr) value represents a lower limit to the total mass loss rate of R99.

A non-spherical stellar wind has been suggested by Leitherer et al. (1994) for the galactic LBV AG Carinae. In this case, the evidence is provided by a high intrinsic polarization of the wind ($\sim$ 0.5%) and by the fact that the wind velocity

measured from UV lines is a factor of two higher than the value obtained from optical spectral features. In particular, the data indicate that the polarization level of AG Carinae, thus its wind geometry, varies over a timescale of 2 months. We suggest that a wind geometry variation similarly occurs in R99, on the basis of the time-variability detected for the Hγ and HeI λ4471 red wings.

An alternative scenario for R99 would be the presence of a binary companion, as earlier suggested by Byrne (1975) and Walborn (1977). However, high resolution echelle spectra by Nota et al. (1996) do not show any velocity structure in the R99 optical lines, similar to the one observed in HD5980 (cf. Barba et al. 1996). Moreover, if we assume that the profile variations in the HeII λ1640, Hγ and HeI λ4471 are due to eclipse, we should be able to simultaneously detect variations in other lines and in the continuum level, which has remained constant over the last 15 years, at least in the UV domain. A possible way to investigate this is the continuous monitoring of absorption lines such as H, He and C features between 3800 Å and 6000 Å in order to measure their radial velocities as a function of time.

Could R99 be defined a LBV? The evidence is, unfortunately, not conclusive. It is also true that no definitive criterion exists to distinguish (dormant) LBVs and non-LBVs. In fact, ultraviolet and optical data indicate that variability occurs in the temperature and wind density of R99 over timescale of one year. Photometric variability has been detected for R99 by van Genderen (1989), who measured a maximum light amplitude of micro-variations (MLA) of 0.12 mag, comparable with the micro-variations observed for LBVs. On the MLA *vs* Spectral type diagram, R99 is located among the S Dor type variables (such as P Cygni, AG Carinae and R71), well distinguished from α Cygni variables. No larger variations have been documented for R99, but it is well known that LBVs may exhibit variations of $\sim$ 1 mag, as in the case of HR Carinae, or be nearly constant over long periods as P Cygni and η Carinae. Line fitting seems to indicate an asymmetric stellar wind in R99, similarly to what has been claimed for AG Carinae by Leitherer et al. (1994). No associated circumstellar nebula has been detected for R99 yet. Although most LBVs appear surrounded by nebulae of stellar origin, there are some LBVs, such as R84 and S Dor, for which associated nebulae have not been resolved yet.

Until more observational evidence is gained on the possible presence of a binary companion, we advocate the two winds model for R99. All the data discussed here are consistent with R99 being a dormant LBV. Of course, a more continuous monitoring at UV and optical wavelengths, together with an extensive polarimetry campaign, is needed in order to properly study the R99 behaviour in the HR diagram.

Acknowledgements. The authors wish to thank Nolan Walborn and Claus Leitherer for many useful discussions and suggestions. They also thank an anonymous referee for improving the manuscript and wish to acknowledge the help from Ralph Bohlin and Randy Thompson in retrieving IUE archive data. AP acknowledges partial support from grant number G005.76100.

References

Barba, R.H. et al. 1996, in Colliding Winds (La Plata 1995), Rev. Mex. Astron. Astrofis. Conf. Ser., in press
Bohannan, B. & Walborn, N.R. 1989, PASP, 101, 520
Byrne, P.B. 1975, Nat, 257, 110
Calvet, N. & Hartmann L. 1992, ApJ, 386, 239
Calvet, N., Hartmann L. & Hewett, R. 1992, ApJ, 386, 229
Crowther, P.A., Hillier D.J., Smith L.J. 1995, A&A, 293, 172
Crowther, P.A. & Smith L.J. 1997, A&A, 320, 500
Davies, R.D., Elliott, K.H. & Meaburn, J. 1976, MNRAS, 81, 89
Doazan, V., Sedmak, G., Barylak, M., Rusconi, L. 1991, "A Be Star Atlas of Far UV and Optical High Resolution Spectra", ESA SP-1147
Dougherty, S.M., Waters, L.B.F.M., Burki, G., Coté, J., Cramer, N., van Kerkwijk, M.H. & Taylor, A.R. 1994, A&A, 290, 609
Drew, J.E., Bunn, J.C. & Hoare, M.G. 1993, MNRAS, 265, 12
Fitzpatrick, E.L. 1986, AJ, 92, 1068
Hamann, W.-R. & Schmutz, W. 1987, A&A, 174, 173
Howarth, I.D. 1983, MNRAS, 203, 301
Humphreys, R.M. & Davidson, K. 1994, PASP, 106, 1025
Langer, N., Hamann, W.-R., Lennon, M., Najarro, F., Pauldrach, A.W.A. & Puls, J. 1944, A&A, 290, 819
Leitherer, C., Allen, R., Altner, B., Damineli, A., Drissen, L., Idiart, T., Lupie, O., Nota, A., Robert, C., Schmutz, W., Shore, S.N. 1994, ApJ, 428, 292
McGregor, P.J., Hyland, A.R. & McGinn, M.T. 1989, A&A, 223, 237
Moorwood, A.F.M., Moneti, A. & Gredel, R. 1991, The Messanger, 63, 77
Morris, P.W., Eenens, P.R.J., Hanson, M.M., Conti, P.S. & Blum, R.D. 1996, ApJ, 470, 597
Nota, A., Pasquali, A., Drissen, L., Leitherer, C., Robert, C., Moffat, A.F.J. & Schmutz, W. 1996, ApJS, 102, 383
Panagia, N., Gilmozzi, R., Macchetto, F., Adorf, H.-M. & Kirshner, R.P. 1991, ApJ, 380, L23
Pasquali, A., Langer, N., Schmutz, W., Leitherer, C., Nota, A., Hubeny, I. & Moffat, A.F.J. 1997, ApJ, 478, 340
Schaerer, D. & Schmutz, W. 1994, A&A, 288, 231
Schmutz, W. 1991, in Stellar Atmosphere: Beyond Classical Models (NATO ASI Series C, Vol. 341), eds. L. Crivillary, I. Hubeny & D.G. Hummer (Dordrecht: Kluver), p.191
Schmutz, W. 1997, in Wolf-Rayet Stars in the Framework of Stellar Evolution, Liege Int. Astroph. Coll. 33, in press
Schmutz, W., Hamann, W.-R. & Wessolowski, U. 1989, A&A, 210, 236
Seaton, M. 1979, MNRAS, 187, 73p
Stahl, O. 1987, A&A, 182, 229
Stahl, O., Wolf, B., Klare, G., Cassatella, A., Krautter, J., Persi, P. & Ferrari-Toniolo, M. 1983, A&A, 127, 49
Stahl, O., Wolf, B., De Groot, M. & Leitherer, C. 1985, A&AS, 61, 237
van Genderen, A.M. 1989, A&A, 208, 135
Walborn, N.R. 1977, ApJ, 215, 53
Walborn, N.R. 1982, ApJ, 256, 45
Walborn, N.R., Nichols-Bohlin, J. & Panek, R.J. 1985, International Ultraviolet Explorer Atlas of O-type Spectra from 1200 to 1900 Å (NASA RP-1155)
Wessolowski, U., Schmutz, W. & Hamann, W.-R. 1988, A&A, 194, 160
Zickgraf, F.J. 1992, in Nonisotropic and Variable Outflows from Stars, eds. L. Drissen, C. Leitherer & A. Nota (San Francisco: ASP), p. 327